

Affine Filter Bank Modulation: A New Waveform for High Mobility Communications

Henrique L. Senger^{*,}, Gustavo P. Gonçalves^{*,}, Bruno S. Chang^{*,},
Hyeon Seok Rou^{†,}, Kuranage Roche Rayan Ranasinghe^{†,},
Giuseppe Thadeu Freitas de Abreu[†] and Didier Le Ruyet[‡]

*CPGEI/Electronics Department, Federal University of Technology - Paraná, Curitiba, Brazil

†School of Computer Science and Engineering, Constructor University, Bremen, Germany

‡CEDRIC/Conservatoire National des Arts et Métiers - Paris, France

Abstract—We propose a new waveform suitable for integrated sensing and communications (ISAC) systems facing doubly-dispersive (DD) channel conditions, as typically encountered in high mobility scenarios. Dubbed Affine Filter Bank Modulation (AFBM), this novel waveform is designed based on a filter-bank structure, known for its ability to suppress out-of-band emissions (OOBE), while integrating a discrete affine Fourier transform (DAFT) precoding stage which yields low peak-to-average power ratio (PAPR) and robustness to DD distortion, as well as other features desirable for ISAC. Analytical and simulation results demonstrate that AFBM maintains quasi-orthogonality similar to that of affine frequency division multiplexing (AFDM) in DD channels, while achieving PAPR levels 3 dB lower, in addition to OOBE as low as -100 dB when implemented with PHYDYAS prototype filters.

I. INTRODUCTION

Next-generation wireless systems are expected to not only enable higher data rates, increase reliability, and provide low latency, but also support many emerging applications, from high-mobility communications [1] to integrated sensing and communications (ISAC) [2]–[4]. High mobility scenarios and/or the higher carrier frequencies required to that end, however, imply the presence of doubly-dispersive (DD) channels, which are known [5] to be challenging to orthogonal frequency division multiplexing (OFDM), the standard waveform used in most modern communications systems, since the large Doppler shifts present in these channels lead to severe inter-carrier interference and consequent link performance degradation.

To overcome this challenge, several novel waveforms have been proposed in the last years [6], with affine frequency division multiplexing (AFDM) being one of the most recent and promising solutions. The AFDM [7] waveform maps data symbols into chirp-based subcarriers in the discrete affine Fourier (DAF) domain, and is capable of attaining full diversity in DD channels via the adjustment of chirp parameters, which are tuned based on the channel characteristics. However, AFDM suffers from a high peak-to-average power ratio (PAPR) and poor spectral containment, leading to challenges in implementation such as inefficient power amplification and high out-of-band emissions (OOBE).

Significant effort has been made recently, therefore, to address these limitations. In [8], for instance, an access scheme was proposed in which the discrete Fourier transform (DFT)

operation of a spread-OFDM system (DFT-s-OFDMA) was replaced by a discrete affine Fourier transform (DAFT), yielding a spread-AFDM access (DAFT-s-AFDM) approach shown to have improved PAPR properties. In turn, in [9] a modified version of orthogonal chirp division multiplexing (OCDM) dubbed c-OCDM was presented, where spectral containment is improved by applying zero-padding in the frequency domain on the chirp matrices prior to modulation. And given that AFDM and OCDM differ mainly on the choice of chirp parameters, the spectral containment approach of [9], it is natural that a similar idea was presented for AFDM in [10], where a modified transceiver structure to reduce the overall computational complexity is also shown.

Approaching the problem from the perspective of OOBE, on the other hand, Filter Bank Multicarrier Modulation (FBMC) emerges as an alternative to design DD-robust ISAC waveforms, due to the per-subcarrier filtering process inherent of filter-bank methods. And while regular FBMC systems are limited to real orthogonality and offset quadrature amplitude modulation (OQAM) modulation to fulfill the Balian-Low theorem, precoded versions such as those proposed in [11]–[14] allow the restoration of complex orthogonality, with additional low PAPR features obtained via DFT-pruning.

In spite of all the aforementioned efforts, the fact is that no ISAC-enabling waveform has been proposed so far that can simultaneously deliver robustness to DD and low PAPR and OOBE. We therefore introduce in this work a novel waveform – referred to as the Affine Filter Bank Modulation (AFBM) – which is designed to address the limitations of existing alternatives all at once. To that end, our proposed waveform in essence integrates a pruned discrete DAFT precoding stage and FBMC filtering to the AFDM scheme. In particular, AFBM achieves low PAPRs close to that of DAFT-s-AFDM, good OOBE characteristics similar to that of FBMC, and quasi-orthogonality in DD channels comparable to that of AFDM.

These claims are demonstrated both via analytical and simulation results, with the remainder of the paper organized as follows. First, the proposed model and the design of AFBM are described in Section II. In Section III simulation results are presented, comparing the performance of the scheme against AFDM in terms of bit error rate (BER), PAPR, and OOBE. Finally, future works and conclusion are offered in Section IV.

II. SYSTEM MODEL AND PROPOSED AFBM DESIGN

A. Transceiver Structure

In a filter bank-based multicarrier system, filtering is performed on each subcarrier, providing a well-localized spectrum, significant rejection of OOB, and the suppression of interference between symbols and between subcarriers.

At the processing stage through the transmitter filter bank, symbols are mapped onto a grid with L subcarriers and K time indices. Then, in order to maintain complex orthogonality, and since half of the system's L subcarriers must be reserved as a guard interval to avoid filter interference, transmission is carried out at a double rate with respect to the conventional transmission seen in OFDM/AFDM systems, namely, every $L/2$ samples.

To facilitate analysis and for clarity of exposition, we will represent the considered system using matrix notation. Let us then define the n -point DFT matrix $\mathbf{F}_n \in \mathbb{C}^{n \times n}$ as

$$\mathbf{F}_n = \left\{ e^{j2\pi kl/n} \right\}_{k,l=0}^{n-1}. \quad (1)$$

The considered filter bank-based system can be characterized as a block structure composed of K symbols with a duration of $T/2$ seconds, where each symbol has L subcarriers spaced by F Hz. Thus, in the TF domain we obtain a grid with L points spaced by F Hz along the frequency axis and K points along the time axis with a space of $T/2$ seconds. In this sense, the total bandwidth is defined as $B = LF$ and the total transmission time interval as $KT/2$.

Next, let $\mathbf{A} \in \mathbb{C}^{L \times K}$ be a matrix containing the symbols in the time-frequency domain. The data symbols are inserted in the first and last $L/4$ positions of the grid according to a pre-established transmission strategy in order to avoid interference from the filter bank (this will be detailed later in the Section), such that the signal after precoding can be expressed as

$$\mathbf{X} = \mathbf{W}_L \text{diag}\{\tilde{\mathbf{b}}\} \mathbf{A}, \quad (2)$$

where $\mathbf{W}_L \in \mathbb{C}^{L \times L}$ represents the L -point DAFT matrix, given by

$$\mathbf{W}_L = \mathbf{\Lambda}_{c_1,L} \mathbf{F}_L \mathbf{\Lambda}_{c_2,L}, \quad (3)$$

where $\mathbf{\Lambda}_{c_i,L} \in \mathbb{C}^{L \times L} = \text{diag}[e^{-j2\pi c_i(0)^2}, \dots, e^{-j2\pi c_i(L-1)^2}]$ is a L -size diagonal chirp matrix with a central digital frequency of c_i while $\tilde{\mathbf{b}} \in \mathbb{C}^{L \times 1}$ is the filter compensation vector.

We emphasize that $\tilde{\mathbf{b}}$ is needed for transceiver complex orthogonality and will also be detailed later in this Section. In addition, the length P of the inverse discrete affine Fourier transform (IDAFT) at the transmitter must be greater than L to prevent the precoding stage DAFT from being nullified by the IDAFT of the filter bank structure.

Finally, the length P must be smaller than the size of the filter bank N so that the chirps are sampled at a rate lower than Nyquist's, allowing frequency containment. From all the above, it follows that the DAFT $\tilde{\mathbf{W}}_P \in \mathbb{C}^{L \times P}$ can be expressed as

$$\tilde{\mathbf{W}}_P = [\mathbf{I}_L \quad \mathbf{0}_{L \times (P-L)}] \mathbf{W}_P. \quad (4)$$

Afterwards, by using frequency domain zero padding, the output matrix \mathbf{Q}_P for a given block can be generated as

$$\mathbf{Q}_P = \mathbf{F}_N^H \mathbf{T} \mathbf{F}_P \tilde{\mathbf{W}}_P^H, \quad (5)$$

where $\mathbf{T} \triangleq [\mathbf{I}_{P,l}^T \quad \mathbf{0}_{(N-P) \times P} \quad \mathbf{I}_{P,u}^T]$, with $\mathbf{T}^T \mathbf{T} = \mathbf{I}_P$, is an $N \times P$ matrix, with $\mathbf{I}_{P,u}$ and $\mathbf{I}_{P,l}$ denoting the first and last $P/2$ columns of the $P \times P$ identity matrix \mathbf{I}_P , respectively.

Considering the transmission of K blocks, the block matrix $\mathbf{Q} \in \mathbb{C}^{NK \times LK}$ is defined as

$$\mathbf{Q} = \mathbf{I}_K \otimes \mathbf{Q}_P, \quad (6)$$

where \otimes refers to the Kronecker product which maps \mathbf{Q}_P to the correct time positions.

Then, the transmitted data can be obtained by convolving the output with the prototype filter impulse response through a Toeplitz filter matrix. Let us consider the diagonal matrix \mathbf{G}_p corresponding to the filter coefficients, that is, $\mathbf{G}_p = \text{diag}(\mathbf{g}_p) \in \mathbb{R}^{N/2 \times N/2}$ for $p = 0, 1, 2, \dots, 2O-1$, where \mathbf{g}_p is given by $\mathbf{g}_p = [g[pN/2], g[pN/2+1], \dots, g[pN/2+N/2-1]]$ and \mathbf{g} is the prototype filter of length ON , where O is the filter overlap factor. Thus, the block Toeplitz filter matrix $\mathbf{G} \in \mathbb{R}^{ON+(K-1)N/2 \times NK}$ can be generated from the vector $[\tilde{\mathbf{G}}_0 \quad \tilde{\mathbf{G}}_1 \quad \tilde{\mathbf{G}}_2 \quad \dots \quad \tilde{\mathbf{G}}_{2O-1}]^T$, namely

$$\mathbf{G} = \begin{bmatrix} \mathbf{G}_0 & \mathbf{0} & \mathbf{0} & \mathbf{0} & \dots & \mathbf{0} \\ \mathbf{0} & \mathbf{G}_1 & \mathbf{G}_0 & \mathbf{0} & \dots & \mathbf{0} \\ \mathbf{G}_2 & \mathbf{0} & \mathbf{0} & \mathbf{G}_1 & \dots & \mathbf{0} \\ \mathbf{0} & \mathbf{G}_3 & \mathbf{G}_2 & \mathbf{0} & \dots & \mathbf{0} \\ \vdots & \mathbf{0} & \mathbf{0} & \mathbf{G}_3 & \dots & \mathbf{0} \\ \vdots & \vdots & \vdots & \vdots & \ddots & \vdots \\ \mathbf{G}_{2O-4} & \vdots & \vdots & \vdots & \ddots & \mathbf{0} \\ \mathbf{0} & \mathbf{G}_{2O-3} & \mathbf{G}_{2O-4} & \vdots & \ddots & \mathbf{G}_1 \\ \mathbf{G}_{2O-2} & \mathbf{0} & \mathbf{0} & \mathbf{G}_{2O-3} & \ddots & \mathbf{0} \\ \mathbf{0} & \mathbf{G}_{2O-1} & \mathbf{G}_{2O-2} & \mathbf{0} & \ddots & \mathbf{G}_3 \\ \vdots & \mathbf{0} & \mathbf{0} & \mathbf{G}_{2O-1} & \ddots & \vdots \\ \vdots & \vdots & \ddots & \vdots & \ddots & \mathbf{0} \\ \mathbf{0} & \mathbf{0} & \dots & \mathbf{0} & \ddots & \mathbf{G}_{2O-1} \end{bmatrix}. \quad (7)$$

Once the transmission matrix has been defined, the output data vector \mathbf{s} of length $M = ON + \frac{N}{2}(K-1)$ is given by

$$\mathbf{s} = \mathbf{G} \mathbf{Q} \mathbf{x} = \tilde{\mathbf{G}} \mathbf{x}, \quad (8)$$

where $\tilde{\mathbf{G}} = \mathbf{G} \mathbf{Q} \in \mathbb{C}^{M \times LK}$ and $\mathbf{x} = \text{vec}(\mathbf{X}) \in \mathbb{C}^{LK \times 1}$.

The symbols are delayed from each other every $N/2$ samples, which the \mathbf{G} structure itself does transparently with the inclusion of matrices $\mathbf{0}_{N/2}$. The representation as a sum of matrices delayed among themselves can be seen in [14].

It can be seen from the above that the proposed structure is an affine-precoded filter bank scheme, which can be implemented efficiently using a polyphase network (PPN) together with an inverse fast Fourier transform (IFFT). Another interpretation is that in the proposed waveform the standard AFDM sinc chirp subcarriers were replaced with chirp filtered ones. The full modulation schematic diagram of the proposed AFBM waveform has been illustrated in Figure 1.

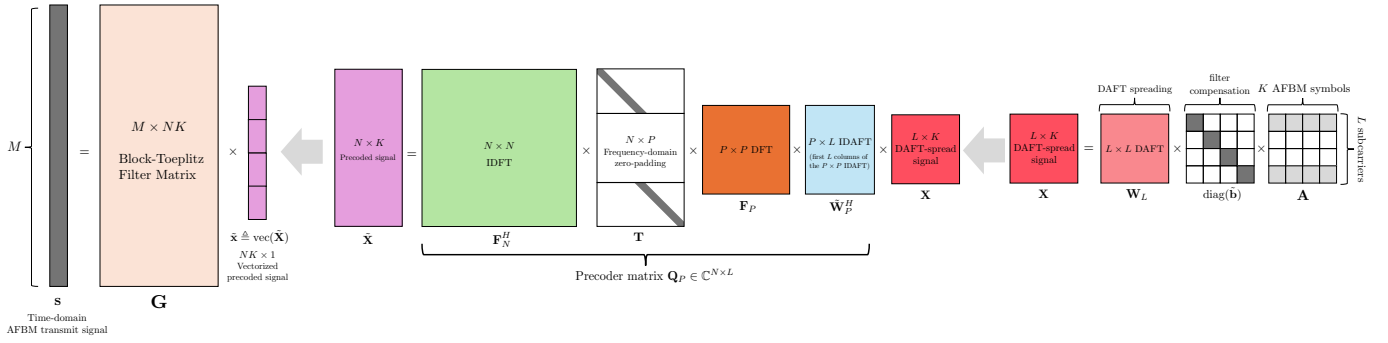


Fig. 1. Illustration of the full AFBM modulation framework.

The signal vector \mathbf{s} is transmitted over a time-varying multipath channel, i.e., the doubly-dispersive channel, described concisely by the circular convolutional matrix form $\mathbf{H} \in \mathbb{C}^{M \times M}$ [12]. Consequently, the received signal $\mathbf{r} \in \mathbb{C}^{M \times 1}$ is expressed by $\mathbf{r} = \mathbf{H}\mathbf{s} + \mathbf{n}$, where \mathbf{n} represents additive white Gaussian noise (AWGN) samples with zero mean and power σ_n^2 . At the receiver, the opposite process to that at the transmitter is carried out.

Firstly, the received signal is demodulated by $\tilde{\mathbf{G}}^H$, generating $\tilde{\mathbf{x}} \in \mathbb{C}^{LK \times 1}$. Then (and considering all time instants), the detected symbols represented by $\tilde{\mathbf{A}} \in \mathbb{C}^{L \times K}$ are obtained through the IDAFT combined with the compensation stage

$$\tilde{\mathbf{A}} = \mathbf{W}_L^H \text{diag}\{\tilde{\mathbf{b}}\} \tilde{\mathbf{X}} \quad (9)$$

where $\tilde{\mathbf{X}} = [\tilde{\mathbf{x}}_0; \tilde{\mathbf{x}}_1; \dots; \tilde{\mathbf{x}}_{K-1}] \in \mathbb{C}^{L \times K}$.

In order to obtain the estimated symbols, the $L/2$ intermediate values between the first and last $L/4$ symbols are discarded, since no data was transmitted in those positions in \mathbf{A} . For symmetry reasons, the compensation stage is used in both the receiver and transmitter. However, it can only be applied to one side effectively.

B. Restoration of Complex Orthogonality

It is possible obtain a filter bank waveform using well localized filters and with complex orthogonality by using the DAFT together with the filter compensation stage to cancel interference. Thus, this part of the precoding presented previously in (2) is defined as

$$\mathbf{C}_f = \mathbf{W}_L \text{diag}\{\tilde{\mathbf{b}}\}, \quad (10)$$

where $\mathbf{C}_f \in \mathbb{C}^{L \times L}$ represents the process within the precoding responsible for restoring complex orthogonality and consists of an L -point DAFT combined with the compensation multiplicative factor.

It follows that in order to preserve complex orthogonality, \mathbf{C}_f must be selected to guarantee the following condition, *i.e.*

$$\mathbf{C}_f^H \mathbf{Q}_P^H \tilde{\mathbf{G}}^T \tilde{\mathbf{G}} \mathbf{Q}_P \mathbf{C}_f \approx \mathbf{U}, \quad (11)$$

where $\mathbf{U} \in \mathbb{R}^{L \times L}$ is a matrix with unit values in the first and last $L/4$ positions of its main diagonal and zeros in the rest. $\tilde{\mathbf{G}}$ represents the filtering corresponding to the

transmission of a single multicarrier symbol, expressed by $\tilde{\mathbf{G}} = [\mathbf{G}_0; \mathbf{G}_1; \dots; \mathbf{G}_{2O-1}] \in \mathbb{R}^{ON \times N}$.

By substituting (10) into (11), the \tilde{l} -th position of $\tilde{\mathbf{b}}$ can be expressed by

$$[\tilde{\mathbf{b}}]_{\tilde{l}} = \begin{cases} \sqrt{\frac{1}{|\tilde{\mathbf{e}}_{\tilde{l}}|}}, & \text{for } \tilde{l} = [0, \dots, \frac{L}{4} - 1; L - \frac{L}{4} - 1, \dots, L - 1] \\ 0, & \text{otherwise} \end{cases} \quad (12)$$

with

$$\tilde{\mathbf{e}} = \text{diag}\{\mathbf{W}_L^H \mathbf{Q}_P^H \tilde{\mathbf{G}}^T \tilde{\mathbf{G}} \mathbf{Q}_P \mathbf{W}_L\}. \quad (13)$$

The compensation stage comprises a multiplicative factor that compensates for the interference in the transmitted symbol that stems from the filter coefficient. The filter coefficients are known, since they come from a pre-established prototype filter [15]. Thus, the objective is to ensure that the filter interference is limited to only one coefficient so that the compensation is done correctly. This is guaranteed by using an overlap factor (O) less than or equal to 1.5 [14]. If the overlap factor is higher than 1.5 the overall response in (11) will have interference components outside the main diagonal, which will reduce the signal-to-interference ratio (SIR).

C. AFBM Effective Channel Analysis

In this section, the effective channel of the AFBM waveform is derived to analyze its robustness in the doubly-dispersive channel, as was proposed for the recently discovered AFDM and OTFS waveforms [6], [7].

To that end, first consider the transmit symbols $\mathbf{A} \in \mathbb{C}^{L \times K}$ reformulated into its vectorized form $\mathbf{a} \in \text{vec}(\mathbf{A}) \in \mathbb{C}^{LK \times 1}$. Then, vectorized form of the DAFT-spread transmit signal $\mathbf{x} \in \mathbb{C}^{LK \times 1}$ is given by

$$\begin{aligned} \mathbf{x} &\triangleq \text{vec}(\mathbf{X}) = \text{vec}\left(\underbrace{\mathbf{W}_L \text{diag}\{\tilde{\mathbf{b}}\}}_{\triangleq \mathbf{C}_f \in \mathbb{C}^{L \times L}} \mathbf{A}\right) \in \mathbb{C}^{LK \times 1} \\ &= \underbrace{(\mathbf{I}_K \otimes \mathbf{C}_f)}_{\triangleq \mathbf{C} \in \mathbb{C}^{LK \times LK}} \cdot \text{vec}(\mathbf{A}) = \mathbf{C} \cdot \mathbf{a}. \end{aligned} \quad (14)$$

Then, following eq. (8), the full AFBM transmit signal in time-domain can be efficiently described in terms of the filter

matrix \mathbf{G} , modified IDAFT matrix \mathbf{Q}_P , and the compensation matrix \mathbf{C}_f leveraging identities involving Kronecker products

$$\begin{aligned} \mathbf{s} &= \mathbf{G}\mathbf{Q}\mathbf{C}\mathbf{a} = \mathbf{G}(\mathbf{I}_K \otimes \mathbf{Q}_P) \cdot (\mathbf{I}_K \otimes \mathbf{C}_f)\mathbf{a} \in \mathbb{C}^{M \times 1} \\ &= \mathbf{G}(\mathbf{I}_K \otimes \mathbf{Q}_P\mathbf{C}_f)\mathbf{a}. \end{aligned} \quad (15)$$

Then, the received signal is given by

$$\mathbf{r} \triangleq \underbrace{\left(\sum_{r=1}^R h_r \Phi_r \mathbf{Z}^{f_r} \mathbf{\Pi}^{\ell_r} \right)}_{\triangleq \mathbf{H}} \mathbf{G}(\mathbf{I}_K \otimes \mathbf{Q}_P\mathbf{C}_f)\mathbf{a}, \quad (16)$$

where $\mathbf{H} \in \mathbb{C}^{M \times M}$ is the doubly-dispersive wireless channel described by R resolvable propagation paths, where each r -th scattering path induces a delay $\tau_r \in [0, \tau^{\max}]$ and Doppler shift $\nu_r \in [-\nu^{\max}, +\nu^{\max}]$ to the received signal, where $\ell_r \triangleq \lfloor \frac{\tau_r}{T_s} \rfloor \in \mathbb{N}_0$ and $f_r \triangleq \frac{N\nu_r}{f_s} \in \mathbb{R}$ are the normalized integer path delay and normalized digital Doppler shift of the r -th propagation path, with sampling frequency $f_s \triangleq \frac{1}{T_s}$.

As elaborated in [6], each r -th path of the full circular convolutional matrix $\mathbf{H} \triangleq \sum_{r=1}^R h_r \Phi_r \mathbf{Z}^{f_r} \mathbf{\Pi}^{\ell_r} \in \mathbb{C}^{M \times M}$, is parametrized by the complex channel fading coefficient $h_r \in \mathbb{C}$, the diagonal prefix phase matrix $\Phi_r \in \mathbb{C}^{M \times M}$ with the IDAFT-based chirp-cyclic prefix phase function $\phi(m) \triangleq c_1(M^2 - 2Mm)$, given by

$$\Phi_r \triangleq \text{diag}[e^{-j2\pi\phi(\ell_r)}, \dots, e^{-j2\pi\phi(1)}, 1, \dots, 1] \in \mathbb{C}^{M \times M}, \quad (17)$$

the diagonal roots-of-unity matrix $\mathbf{Z} \in \mathbb{C}^{M \times M}$ given by

$$\mathbf{Z} \triangleq \text{diag}[e^{-j2\pi\frac{0}{M}}, \dots, e^{-j2\pi\frac{M-1}{M}}] \in \mathbb{C}^{M \times M}, \quad (18)$$

which is taken to the f_r -th power, and the right-multiplying circular left-shift matrix $\mathbf{\Pi} \in \mathbb{C}^{M \times M}$. In all, this channel matrix composes of R shifted diagonals whose position is dependent on the normalized path delay, and coefficients dependent on the normalized Doppler shift of the path.

For the sake of analyzing the properties of the effective channel with respect to the double dispersivity, i.e., the effect of delay and Doppler of each path unto the channel structure, let us simplify without loss of generality, by considering only one AFBM symbol, $K = 1$, such that the Kronecker products with the identity matrix \mathbf{I}_K are reduced.

Furthermore, the effective channel \mathbf{H}_{eff} will be defined as the full transformation matrix only between the DAFT-spread signal \mathbf{x} and the demodulated signal $\tilde{\mathbf{x}}$, i.e., without de-spreading and filter compensation, as these operations do not alter the properties of the waveform over the core doubly-dispersive channel operations by the modulating DAFT/IDAFT \mathbf{Q}_P .

Then, including the corresponding demodulation and equalization, the effective doubly-dispersive channel matrix of the AFBM waveform is defined as

$$\mathbf{H}_{\text{eff}} \triangleq \mathbf{Q}_P^H \mathbf{G}^H \left(\sum_{r=1}^R h_r \Phi_r \mathbf{Z}^{f_r} \mathbf{\Pi}^{\ell_r} \right) \mathbf{G} \mathbf{Q}_P \in \mathbb{C}^{L \times L}, \quad (19)$$

which captures the structure of the doubly-dispersive channel after the filter shaping and the truncated IDAFT/DAFT.

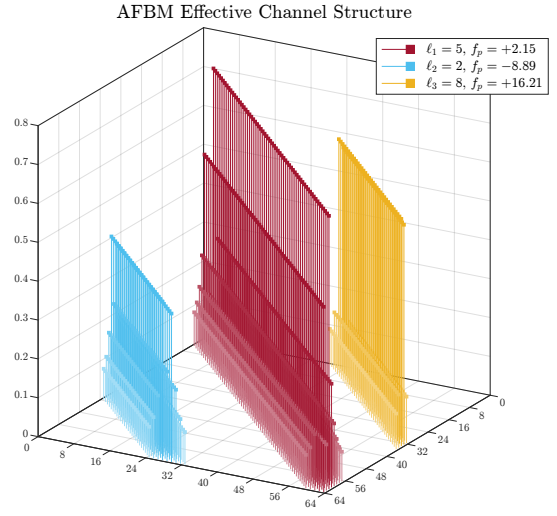


Fig. 2. 3D illustration of a three-path AFBM effective channel of the DAFT-spread signal, where the normalized delay and Doppler shifts are denoted in legend. The AFBM parameters are $L = 64$, $N = 128$, $P = 128$, $O = 4$ with the PHYDYAS4 prototype filter.

This AFBM effective channel has been illustrated in Fig. 2 for a scenario with three distinct propagation paths, where the spreading of the band-diagonals of the effective channel is observed. This behavior is alike to the AFDM waveform [6], [7] inherently due to the IDAFT-based modulation process – except for the different sideband behavior from the filter design – resulting in a deterministic shift of the diagonals based on the path delay and Doppler shift indices, which is the key factor enabling the robustness of the waveform by mitigating inter-path interference, in addition to the highly beneficial implications to ISAC parameter estimation. In other words, the proposed AFBM enables robust communications over doubly-dispersive channels alike to the AFDM.

III. SIMULATION RESULTS

In this section, simulation results presenting PAPR and OOB of the proposed scheme will be shown, together with a comparison taking into account the classical AFDM scheme. For these simulations, the total number of subcarriers L is 128, the chirp size P is 192 and the filter bank DFT size N is 256.

Each transmission was composed of $K = 8$ symbols, with a carrier frequency f_c of 4 GHz. The channel is a doubly dispersive one, with three resolvable paths and corresponding normalized delays and digital Doppler shifts. We recall that the chirp frequencies for each (I)DAFT were chosen to uphold the orthogonality condition [6] $2(f^{\max} + \xi)(\ell^{\max} + 1) + \ell^{\max} \leq P$, where f^{\max} and ℓ^{\max} are, respectively, the maximum normalized digital Doppler shift and delay of the channel and $\xi \in \mathbb{N}_0$ is a free parameter determining the so-called guard width, denoting the number of additional guard elements around the diagonals to anticipate for Doppler-domain interference.

Figure 3 presents PAPR results from the considered systems. It can be seen that, due to its single-carrier like structure, the proposed structure has an advantage of 2 dB with respect to

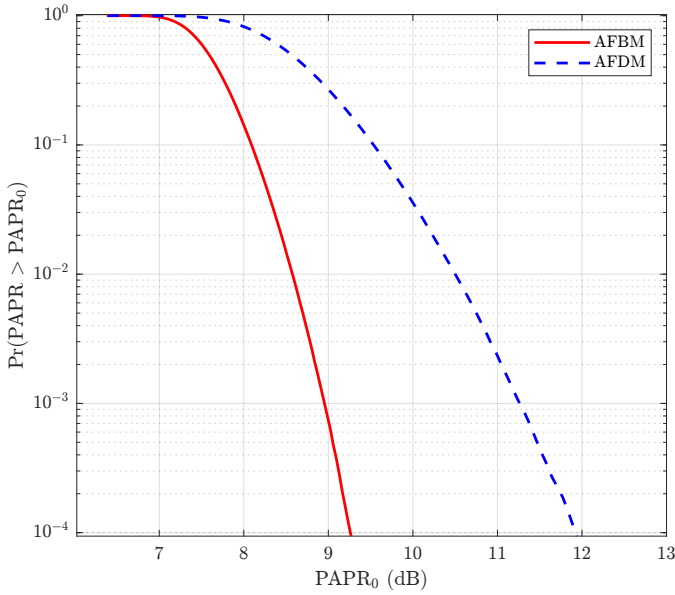


Fig. 3. PAPR performance of AFDM and AFBM.

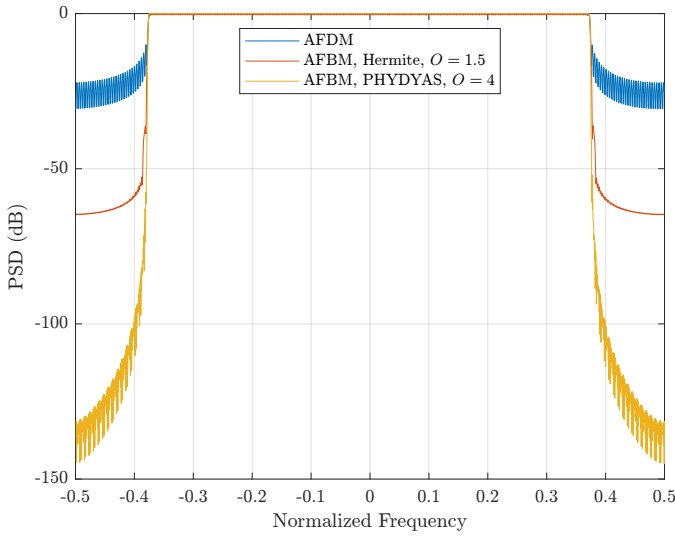


Fig. 4. OOB Performance of AFDM and AFBM with the Hermite and PHYDYAS prototype filters.

regular AFDM, which has the same high PAPR of regular OFDM-based schemes. Also, since the proposed scheme can be seen as an affine version of the pruned DFT spread FBMC, the low PAPR characteristic of the original version is maintained.

The OOB of the considered schemes are shown in Figure 4. In this scenario, two prototype filters were considered for AFBM: the truncated Hermite (with $O = 1.5$) and the full PHYDYAS (with $O = 4$). Due to the usage of well-localized filters instead of the rectangular window there is a significant advantage in OOB of the AFBM system with respect to regular AFDM. Here, an interesting compromise regarding the prototype filter choice appears: if lower overall latency is prioritized a shorter filter can be selected, at the expense of

worse (but still much better than AFDM) spectral localization. Finally, we remember that if the nonlinear characteristics of high power amplifiers are considered, the good OOB characteristics of the proposed waveform will not be severely affected due to the low PAPR.

IV. CONCLUSION

We introduced an affine-coded filter bank scheme called AFBM in this work. It was seen that it has lower PAPR and OOB than regular AFDM. In the follow-up, new detection structures taking into account the interference introduced by prototype filters with high overlap factors and simplified structures to reduce the overall computational complexity will be proposed. Moreover, the sensing performance of this scheme will be investigated. Furthermore, adapted channel estimation schemes for the proposed waveform will be proposed, as well as studies dealing with its robustness to high mobility conditions. Finally, chirp parameters optimization to reduce even further the PAPR will be developed.

REFERENCES

- [1] J. Wu and P. Fan, "A survey on high mobility wireless communications: Challenges, opportunities and solutions," *IEEE Access*, vol. 4, pp. 450–476, 2016.
- [2] Z. Wei *et al.*, "Integrated sensing and communication signals toward 5G-A and 6G: A survey," *IEEE Internet of Things Journal*, vol. 10, no. 13, 2023.
- [3] N. González-Prelcic *et al.*, "The integrated sensing and communication revolution for 6G: Vision, techniques, and applications," *Proceedings of the IEEE*, vol. 112, no. 7, 2024.
- [4] K. R. R. Ranasinghe *et al.*, "Joint channel, data, and radar parameter estimation for afdm systems in doubly-dispersive channels," *IEEE Transactions on Wireless Communications*, vol. 24, no. 2, 2025.
- [5] J. Du and S. Signell, "Comparison of CP-OFDM and OFDM/OQAM in doubly dispersive channels," in *Future Generation Communication and Networking (FGCN 2007)*, vol. 2, 2007.
- [6] H. S. Rou *et al.*, "From orthogonal time–frequency space to affine frequency-division multiplexing: A comparative study of next-generation waveforms for integrated sensing and communications in doubly dispersive channels," *IEEE Signal Process. Mag.*, vol. 41, no. 5, 2024.
- [7] A. Bemani, N. Ksairi, and M. Kountouris, "Affine frequency division multiplexing for next generation wireless communications," *IEEE Transactions on Wireless Communications*, vol. 22, no. 11, 2023.
- [8] Y. Tao *et al.*, "DAFT-spread affine frequency division multiple access for downlink transmission," in *GLOBECOM 2024 - 2024 IEEE Global Communications Conference*, 2024.
- [9] M. S. Omar and X. Ma, "Spectrum design for orthogonal chirp division multiplexing transmissions," *IEEE Wireless Communications Letters*, vol. 9, no. 11, 2020.
- [10] V. Savaux, "Special cases of DFT-based modulation and demodulation for affine frequency division multiplexing," *IEEE Transactions on Communications*, vol. 72, no. 12, 2024.
- [11] R. Zakaria and D. Le Ruyet, "A novel filter-bank multicarrier scheme to mitigate the intrinsic interference: Application to mimo systems," *IEEE Transactions on Wireless Communications*, vol. 11, no. 3, 2012.
- [12] R. Nissel and M. Rupp, "Pruned DFT-spread FBMC: Low PAPR, low latency, high spectral efficiency," *IEEE Transactions on Communications*, vol. 66, no. 10, 2018.
- [13] R. P. Junior, C. A. F. d. Rocha, B. S. Chang, and D. Le Ruyet, "A novel DFT precoded filter bank system with iterative equalization," *IEEE Wireless Communications Letters*, vol. 10, no. 3, 2021.
- [14] —, "A generalized DFT precoded filter bank system," *IEEE Wireless Communications Letters*, vol. 11, no. 6, 2022.
- [15] —, "A two-dimensional FFT precoded filter bank scheme," *IEEE Transactions on Wireless Communications*, vol. 22, no. 11, 2023.